https://doi.org/10.5194/egusphere-2026-159
Preprint. Discussion started: 2 February 2026

A high-resolution snow dataset for Switzerland (2016–2025) combining physics-based simulations and in situ observations

Moritz Oberrauch[1,2], Bertrand Cluzet[1], Jan Magnusson[1], Giulia Mazzotti[1,3], Rebecca Mott[1], Louis Quéno[1], Clare Webster[1,4], Tobias Zolles[1], and Tobias Jonas[1]

[1]WSL Institute for Snow and Avalanche Research SLF, Davos, Switzerland
[2]Department of Civil, Environmental and Geomatic Engineering, ETH Zürich, Switzerland
[3]Université Grenoble Alpes, INRAE, CNRS, IRD, Grenoble INP, IGE, Grenoble, France
[4]Department of Geography, University of Zurich, Zürich, Switzerland

Correspondence: Moritz Oberrauch (moritz.oberrauch@slf.ch)

Abstract. We present a high-resolution snow dataset that provides daily estimates of snow depth, snow water equivalent, snow cover fraction, and snowmelt runoff for Switzerland and hydrologically connected bordering regions, covering water years 2016 to 2025. The dataset is based on fully distributed simulations at 250 m resolution using the multi-layer, physics-based snow model FSM2OSHD, operated by the Swiss Operational Snow Hydrological Service. To capture the high spatial heterogeneity of snow cover dynamics in complex mountainous terrain, the modeling framework combines dedicated dynamical and statistical downscaling of numerical weather prediction data with the upscaling of hyper-resolution terrain, forest, and light-availability datasets, explicitly accounting for subgrid variability. The particle filter-based assimilation of in situ snow depth observations from 444 monitoring stations across the domain dynamically corrects spatiotemporal error patterns in the meteorological forcing data. This approach ensures consistent input data quality over the entire 10-year period and mitigates potential discontinuities caused by changes within the numerical weather prediction system. Example applications demonstrate the dataset's ability to capture regional and interannual variability of snow water resources, snow cover extent, and snow duration. With 10 years of physically consistent estimates at high spatial and temporal resolution, this dataset represents, to our knowledge, the most accurate and comprehensive record of snow cover dynamics for Switzerland to date. It expands the snow data record for the European Alps and bridges the gap between coarse global reanalyses and detailed local observations. The dataset is publicly and freely available providing a valuable resource for a wide range of scientific and applied studies in hydrology, ecology, climate, and cryospheric research.

1 Introduction

Seasonal snow drives numerous hydrological and ecological processes (Han et al., 2024; Hale et al., 2023; Slatyer et al., 2022) and affects many socioeconomic aspects (Rasul and Molden, 2019). Snow-cover extent, as well as timing and intensity of snowmelt, have a direct impact on avalanche and flood hazards (Musselman et al., 2018; Li et al., 2019; Eckert et al., 2024), freshwater availability (Musselman et al., 2021; Siirila-Woodburn et al., 2021), hydropower production (Magnusson et al., 2020; Hou et al., 2025), and winter tourism (Moreno-Gené et al., 2018; Morin et al., 2021). However, estimating snow water

https://doi.org/10.5194/egusphere-2026-159
Preprint. Discussion started: 2 February 2026

resources in mountainous regions is particularly challenging due to the substantial spatial variability of the terrain and the snowpack (Grünewald et al., 2010; López-Moreno et al., 2013; Mott et al., 2018), the lack of accurate distributed measurements (Dozier et al., 2016; Gascoin et al., 2024), and the uncertainties inherent in snowpack estimated from numerical models (Menard et al., 2021).

The mountain snowpack remains severely undersampled despite continuous monitoring efforts (Largeron et al., 2020). Detailed, high-resolution hydrometeorological and snow datasets exist for small Alpine catchments, such as the Dischma catchment in Switzerland (Magnusson et al., 2025) or the Izas catchment in the Spanish Pyrenees (Revuelto et al., 2017), but their spatial coverage is limited. Similarly, airborne lidar- or photogrammetry-based snow depth maps are available only for a few select catchments and at specific times during the season (Painter et al., 2016; Bührle et al., 2023). For larger scales and with roughly weekly temporal resolution, spaceborne optical sensors provide observations of snow cover extent and snow cover fraction (SCF) (Gascoin et al., 2019), but cannot provide direct information on snow depth or snow water equivalent (SWE). The NorSWE dataset (Mortimer and Vionnet, 2025) compiles SWE observations from more than 10,000 locations across the Northern Hemisphere over three decades, with the Alps represented by manual point measurements from 11 sites in Switzerland only. Spatially explicit snow depth observations from Sentinel-1 retrievals are possible under dry-snow conditions (Lievens et al., 2019, 2022), but truly reliable, high-resolution, spatiotemporally continuous SWE estimates remain elusive (Gascoin et al., 2024; Mortimer et al., 2020). While numerical models can provide such continuous estimates at any desirable spatial and temporal resolution, they are subject to inherent uncertainties in the parametrization and forcing data (Günther et al., 2019; Menard et al., 2021).

Reanalysis products provide estimates of past states by constraining numerical simulations through the assimilation of observational datasets. While global reanalyses within numerical weather prediction (NWP) systems, such as ECMWF's ERA5 (Hersbach et al., 2020), are widely used for climate monitoring, their snow-related variables offer only low resolution and accuracy in mountainous regions (Li et al., 2022; Monteiro and Morin, 2023; Kouki et al., 2023). Fiddes et al. (2019) presented an efficient method that couples sub-grid clustering of complex terrain, downscaling of global meteorological reanalysis data, and the assimilation of spaceborn SCF observations, to enable high-resolution ensemble-based snow reanalyses in mountain regions. Other recent efforts in the snow modeling community have produced detailed and dedicated long-term snowpack reanalysis datasets: the modeling and data assimilation system SNODAS provides daily snowpack and precipitation data at 1 km resolution over the contiguous United States from 2003 onward (Barrett, 2003); daily estimates of SWE and SCF based on the assimilation Landsat SCF observations into a land surface model, coupled with a snow depletion curve, are available for the Sierra Nevada (Margulis et al., 2016) and the western United States (Fang et al., 2022), at a resolution of 90 m and 500 m, respectively; a similar dataset based on the joint assimilation of Landsat and MODIS SCF observations is available for High Mountain Asia (Liu et al., 2021); a daily 10 km gridded snow depth and SWE estimates over the Iberian Peninsula since 1980 are available based on the physics-based snow model FSM forced with downscaled ERA-interim data (Alonso-González et al., 2018, and references therein); daily 1 km gridded estimates of snow depth and snow cover duration between 1961 and 2020 are available for Austria, based on simulations of the SNOWGRID model in a climate configuration forced with gridded meteorological observatiions (Olefs et al., 2020); the IT-SNOW reanalysis provides daily estimates of snow states for Italy

https://doi.org/10.5194/egusphere-2026-159
Preprint. Discussion started: 2 February 2026

from water year 2010 onward by combining model simulations with in-situ and spaceborne osbervations (Avanzi et al., 2023); the S2M meteorological and snow cover reanalysis combines the meteorological analysis SAFRAN and the high complexity snow model CROCUS within the SURFEX/ISBA land surface model, covering the semi-distributed massifs of the French Alps, Pyrenees, and Corsica from 1958 onwards (Vernay et al., 2022, and references therein).

Here, we present a continuous 10-year snow reanalysis dataset for Switzerland and hydrologically connected bordering regions, produced within the near-real-time modeling framework of the Swiss Operational Snow Hydrological Service (OSHD). The dataset provides daily estimates of snow depth, SWE, SCF, and snowmelt runoff by combining high-resolution simulations from the intermediate-complexity, physics-based snow model FSM2OSHD (Mott et al., 2023) with in situ snow depth observations from 444 stations (Oberrauch et al., 2024). To capture the high spatial variability of snow processes in complex Alpine terrain, the modeling chain employs dedicated dynamical and statistical downscaling of NWP forcing data to a spatial resolution of 250 m, solves the coupled mass- and energy-balance equation for multiple numerical snow layers, and explicitely accounts for differences in the atmospheric and snowpack procsesses of open, forested, and glaciated areas (Mazzotti et al., 2021). The simulations are based on upscaled versions of the most accurate hyper-resolution datasets currently available, including a 10 m digital elevation model and terrain surface model (swissALTIRegio, 2025; swissSurface3D, 2025), as well as light availability maps that resolve terrain and vegetation shading down to individual trees for every hour of the year (Webster et al., 2025). Temporal consistency across the whole period is ensured through an assimilation scheme that homogenizes meteorological inputs despite changes in the source and processing level of the forcing data (Oberrauch et al., 2025; MeteoSwiss, 2024). The model has been tuned and validated continuously over the past decade against snow depth, SWE, SCF, and new snow observations from a dense station network (Mott et al., 2023; Cluzet et al., 2024; Haagmans et al., 2025).

To our knowledge, this dataset represents the most accurate and comprehensive snow reanalysis for Switzerland to date. By providing 10 years of physically consistent estimates of snow cover dynamics at a subkilometric resolution across a large part of the European Alps, it contributes to the snow database of a region characterized by highly complex terrain and diverse hydroclimatic regimes. The dataset helps bridge existing scale and knowledge gaps between coarse global products (e.g., Hersbach et al., 2020) and detailed local observations (e.g., Magnusson et al., 2025) and provides a robust foundation for hydrological, ecological, and cryospheric analyses (e.g., Jenicek et al., 2016; Xie et al., 2018; Floriancic et al., 2020; Publications Office of the European Union, 2023). The data is publicly and freely available under https://zenodo.org/records/17313889?preview=1&token=eyJhbGciOiJIUzUxMiJ9.eyJpZCI6IjhkOTgwNDcyLWI3ZWYtNGZmOS1iY2VkLTFjZTkyMmNmMzFhZCIsImRhdGEiOnt9LCJyYW5kb20iOiI2ZTEwZjVhZDdmNGZlZWE2NjIyYjBlMzkzM2M2NGFmMyJ9.cu88BUCkEuh0UH37WTvSZTIbDiqw331U6yF7T51TbhQMUvOv4pmmrA2bN2LEs6NJhW1Pp4Zdm7BTqNUvU0O7Lw (Oberrauch et al., 2026), offering substantial value to a wide range of scientific and applied users.

2 Data and model chain

The basis for the presented dataset is the fully distributed, physics-based, multi-layer snow model FSM2OSHD (Mott et al., 2023), operated by the OSHD. Forcing data from the Federal Office of Meteorology and Climatology, MeteoSwiss, are debiased

https://doi.org/10.5194/egusphere-2026-159
Preprint. Discussion started: 2 February 2026

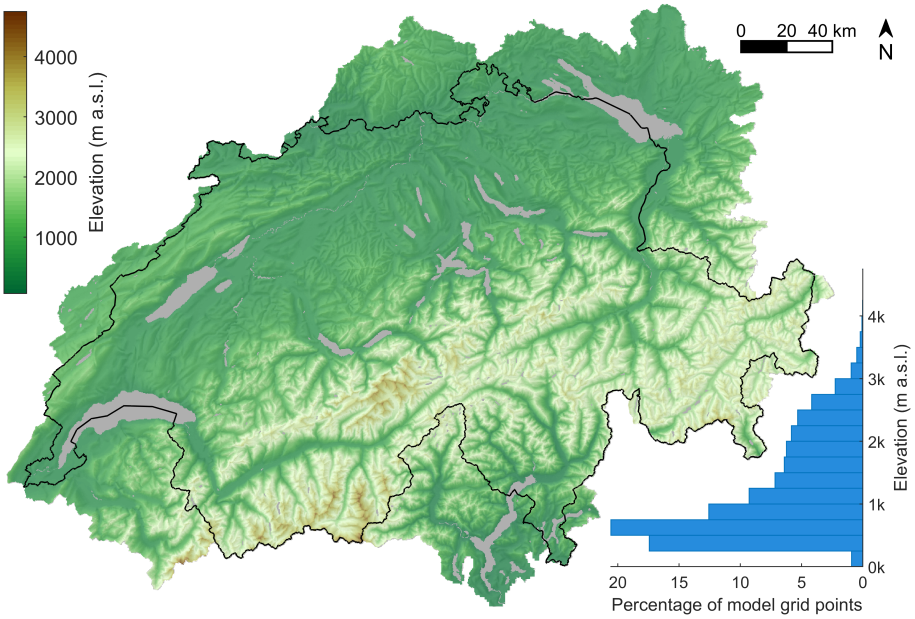

Figure 1. Terrain representation of the model domain based on the 250 m resolution digital elevation model. Major water bodies are shown in grey, the Swiss national border is outlined in black, and a shaded relief is used as a background map. The panel on the bottom right shows the distribution of model grid elevations in 250 m bands.

and downscaled to the 250 m model resolution and dynamically corrected through the assimilation of in situ snow depth observations (Oberrauch et al., 2024). The following section provides a brief overview of the study area, the datasets used, the modeling chain, and the particle filter (PF) based assimilation scheme.

2.1 Study area

The presented dataset spans Switzerland and hydrologically connected neighboring regions of Austria, France, Germany, Italy, and Liechtenstein. The model domain has a latitudinal and longitudinal extent of 272 km and 365 km, respectively. It comprises 928 155 grid cells at a spatial resolution of 250 m, for a total area of over 58 000 km^2. Model elevations range from 180 m a.s.l. to 4750 m a.s.l., with 50 % of the grid points located above 966 m a.s.l.. Roughly 40 % of the domain is forested, with forest cover extending up to 2 400 m a.s.l., although less than half of the forest is situated above 1 000 m a.s.l. (Szerencsits, 2012; Haagmans et al., 2025).

Switzerland lies in Central Europe and spans both sides of the European Alps and the adjacent lowlands, each characterized by distinct hydroclimatic regimes. The main Alpine ridge forms a climatic divide between Mediterranean air masses to the south and Atlantic air masses to the north (Gubler et al., 2023). Precipitation is generally high in the Alps, the Alpine foothills, and the Jura mountains (in the northwest of the country), with annual totals of around 2 000 mm. In contrast, certain inner-Alpine valleys are sheltered from moist air masses and are therefore comparatively dry, with annual totals of about 700 mm

https://doi.org/10.5194/egusphere-2026-159
Preprint. Discussion started: 2 February 2026

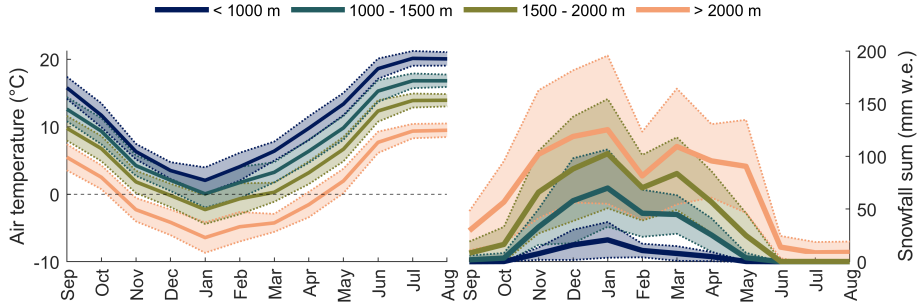

Figure 2. Monthly climatology of near-surface air temperature (left) and snowfall sums (right) stratified by elevation bands over the period between September 2015 and August 2025, based on the meteorological forcing data. Results are averaged over all model grid points within the respective elevation bands. Solid lines represent mean values, while the shading indicates the standard deviation across the 10 seasons.

or less (MeteoSwiss, 2025). Figure 2 displays average monthly air temperature and solid precipitation aggregated into four elevation bands, based on the forcing data over the presented 10-year period (with the interannual variability indicated by shadings).

2.2 Used datasets

MeteoSwiss officially replaced its operational forecasting model in June 2024 (MeteoSwiss, 2024), shifting from COSMO (Baldauf et al., 2011) to ICON (Zängl et al., 2015) as the dynamical core. Moreover, ICON data was reprocessed for a transitional period between 2020 and 2024. ICON is the higher-resolution successor to COSMO, and provides an improved representation of terrain-induced variability (Zängl et al., 2015; MeteoSwiss, 2023). Hence, for the water years 2016 to 2020, we use analysis data from COSMO, while from 2021 onward, ICON data were employed at different processing levels: (re-)forecast data for the water years 2021 to 2023 and analysis data from 2024 onward. Oberrauch et al. (2025) demonstrated that correcting spatiotemporal error patterns in the forcing data through the assimilation of point observations homogenizes snow model performance. Thereby, potential temporal discontinuities arising from changes in the forcing data sources are mitigated, as detailed below in Section 2.4.

The hourly NWP data are downscaled from 1 km to the 250 m model resolution using various statistical and dynamic downscaling schemes (detailed below in Section 2.3), all based on a detailed land-use and land-cover dataset. The basis is the swissALTIRegio digital elevation model (DEM) with a resolution of 10 m (swissALTIRegio, 2025), used to compute the 250 m model DEM, as well as the topographic position index, slope, aspect, and subgrid terrain variability for each grid cell. The CORINE land cover dataset (European Union's Copernicus Land Monitoring Service information, 2020) was used to distinguish between open, forested, and glaciated areas, which are handled differently by the FSM2OSHD model (detailed below in Section 2.3). Large water bodies where snow does not accumulate are excluded from the domain, indicated as grey areas in Figure 1 and subsequent figures.

https://doi.org/10.5194/egusphere-2026-159
Preprint. Discussion started: 2 February 2026

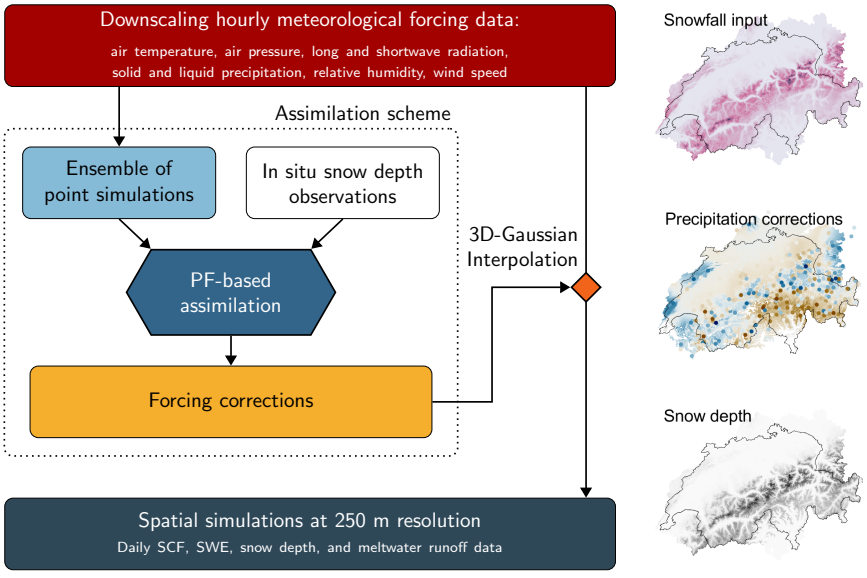

Figure 3. Simplified flowchart of the modeling chain, including the PF-based assimilation scheme to correct meteorological forcing inputs.

The SwissRad10 dataset provides domain-wide estimates of direct and diffuse radiation at 10 m resolution across Switzerland, accounting for vegetation and terrain shadowing as well as the sky view fraction (Webster et al., 2025). The dataset is derived from high-resolution airborne lidar data that resolves individual trees (swissSurface3D, 2025), using the Canopy Radiation Model (Webster et al., 2023). It provides terrain-only and leaf-on and leaf-off canopy scenarios (of which only the latter is used in FSM2OSHD) at hourly resolution over a full annual solar cycle.

2.3 The OSHD modeling chain

FSM2OSHD is a multi-layer, physics-based model solving the coupled mass and energy balance for individual numerical snow layers at an hourly resolution, without directly accounting for snow microstructures and metamorphism (Mott et al., 2023). FSM2OSHD was originally based on the Flexible Snow Model (FSM2, Essery, 2015; Essery et al., 2025), incorporating additional process-based refinements adapted and tuned for the application within the OSHD.

The implemented snowpack process parameterizations (FSM2OSHD code available at https://github.com/oshd-slf/FSM2oshd) are briefly outlined below; please refer Mott et al. (2023, and references therein) for more detailed information. Fresh snow density is estimated from air temperature and wind speed during the snowfall (Vionnet et al., 2012), fine-tuned against observations of fresh snow fallen and settled over a period of 24 hours. The settling of the snowpack and the associated changes in snow density are computed via a viscosity-based overburden scheme adapted from Vionnet et al. (2012). Increasing snow weight compresses the underlying layers depending on the layer's viscosity, which, in turn, depends on layer density, temperature, and liquid water content. Thermal conductivity between snow layers is diagnosed from snow density (Douville

https://doi.org/10.5194/egusphere-2026-159
Preprint. Discussion started: 2 February 2026

et al., 1995; Essery, 2015), while the ground heat flux is estimated using a five-layer soil model (Cox et al., 1999; Essery, 2015). Turbulent fluxes at the snow–atmosphere boundary are parameterized following Essery (2015, Section 2.3.4), with transfer coefficients adjusted according to the Richardson number (Ri, Louis, 1979) and capped at $Ri = 0.2$ to prevent an unrealistic stability-induced shutdown of the turbulent exchange. Liquid water retention in each layer follows a bucket-storage approach, whereby the storage capacity depends on snow density (Anderson, 1976; Boone and Etchevers, 2001). Broadband snow albedo is computed with a snow-age-dependent decay function, following a linear rate for cold snow and an exponential rate for melting snow (Douville et al., 1995). Albedo values are reset to their maximum fresh-snow values after a minimum of 10 mm w.e. new snow accumulation over 24 hours. Additional tuning accounts for bare ground piercing through thin snowpacks, as well as aspect- and slope-dependent differences in the albedo decay based on a comparison with spaceborne snow wetness and SCF observations (Cluzet et al., 2024). SCF in open, non-forested areas is estimated by tracking the seasonal evolution of snow depth and SWE depending on subgrid terrain variability (Helbig et al., 2021), while a simpler hyperbolic tangent model is applied within forests (Essery, 2015).

FSM2OSHD differentiates between open, forested, and glaciated terrain by simulating the snow cover separately for each land cover type and aggregating the results as a weighted average according to the respective land cover fractions within each grid cell. Glaciated terrain is simulated analogously to open terrain but with a modified ground heat flux and roughness length. For forest-covered grid cells, FSM2OSHD explicitly accounts for key snow–canopy and canopy–atmosphere interactions, including snowfall interception, snow unloading and sublimation from the canopy, shortwave radiation transmission, longwave radiation enhancement, and wind attenuation (Mazzotti et al., 2020a, 2021; Essery et al., 2025). Forest processes and vegetation shading extend beyond the forest edges, thereby influencing adjacent open terrain.

The hourly NWP data is bias corrected and downscaled to the 250 m model grid and station locations (see Section 4 and Table 1 in Mott et al., 2023) by statistically downscaling the wind fields (Winstral et al., 2017), dynamically downscaling the radiation input (Jonas et al., 2020; Webster et al., 2025), and linearly interpolating air temperature, relative humidity and precipitation with corresponding lapse rate corrections. Slope-dependent precipitation adjustment accounts for not explicitly resolved redistribution processes in mountainous terrain. (Griessinger et al., 2016). For ICON data, we use the provided solid and liquid precipitation fractions, while COSMO precipitation data are partitioned into rain and snow based on air temperature (Kavetski and Kuczera, 2007; Magnusson et al., 2014; Oberrauch et al., 2024). This partitioning also enables the assimilation scheme to modify the precipitation phase through small adjustments in air temperature (detailed below in Section 2.4).

Analogous to the operational products of the OSHD, the presented dataset represents seasonal snow for individual water years, defined as the period from September 1 to August 31 of the following year. Accordingly, at the beginning of each water year, all snow is removed, disregarding the buildup of any perennial snow and firn at high elevations and on glaciers. A one-year spin-up simulation is performed to initialize the soil layer temperatures for the water year 2016. Subsequently, the end-of-season soil temperatures are used to initialize the following season.

https://doi.org/10.5194/egusphere-2026-159
Preprint. Discussion started: 2 February 2026

2.4 PF-based assimilation

The particle filter (PF, Chopin and Papaspiliopoulos, 2020) is a Bayesian data assimilation method that estimates the state of a system from a weighted set of ensemble members, referred to as particles. The ensemble simulation represents the initial uncertainty of the prior estimate. Particle weights are sequentially updated based on the likelihood of the given observation, under the assumption that the respective particle represents the true state of the system. The resulting posterior distribution combines prior information and observations, accounting for their respective uncertainties. Particles are propagated from one assimilation step to the next according to the model dynamics, with a potential resampling step to ensure adequate dispersion. Given spatially correlated priors, it is possible to update unobserved locations indirectly (e.g., Odry et al., 2022; Alonso-González et al., 2023).

We employ the PF-based assimilation scheme described by Oberrauch et al. (2024) to correct spatiotemporal error patterns in the meteorological forcing data by assimilating point snow depth observations from 444 stations across the domain. Local corrections are inferred independently for each station location and three-day assimilation window, and subsequentially interpolated to unobserved locations across the domain. The assimilation procedure is performed on a separate "offline" set of point simulations, allowing for computationally efficient updates of the fully distributed simulations over such a large domain without the need for a gridded ensemble.

The prior ensemble is generated by stochastically perturbing incoming longwave radiation and air temperature additively, and precipitation amount multiplicatively via a scaling factor. The additive perturbations and scaling factors are drawn from normal and lognormal distributions, respectively, all centered around the non-perturbed state. This perturbation strategy provides direct and largely independent handles on the radiative energy budget, as well as the amount and phase of precipitation (the latter via small perturbations of air temperature), thereby minimizing equifinality issues (Oberrauch et al., 2024). Best results were achieved by allowing sufficient flexibility in correcting the given forcing variables, which was accomplished by defining less constrained perturbation priors. The additional perturbation of model parameters, namely the snow viscosity, did not notably improve the final estimate (Oberrauch et al., 2025). Hence, to create this dataset, we applied the "METEO" perturbation strategy from Oberrauch et al. (2025), which draws perturbations from more relaxed prior distributions and assumes an observation error of 5 % of the observed snow depth, with bounds of 5 and 20 cm. Further details are given in Section 2.8 and Tables 2 and 3 of Oberrauch et al. (2025).

For each station and assimilation window, a set of optimal forcing corrections is defined based on the probability density distribution of the perturbation posterior. At the end of each three-day assimilation window, the posterior distribution is computed from the weight of each particle ω^i based on the difference between simulated snow depth d^i_{sim} and observed value d_{obs}:

$$\omega^i = \exp\left(-0.5\left(\frac{d^i_{\text{sim}} - d_{\text{obs}}}{\sigma_{\text{obs}}}\right)^2\right), \tag{1}$$

whereby σ_{obs} represents the observation uncertainty. The most conservative local mode of the resulting multivariate distribution, i.e., the point with the highest probability density closest to the unperturbed state, is chosen as the optimal set of forcing

https://doi.org/10.5194/egusphere-2026-159
Preprint. Discussion started: 2 February 2026

corrections. For a more in-depth explanation, please refer to Oberrauch et al. (2024, Section 2.4.1). This deliberate collapse of the probabilistic information onto a deterministic estimate forms the basis for the subsequent propagation of the inferred information to unobserved locations.

The independently inferred local forcing corrections are interpolated in space via a three-dimensional Gaussian interpolation scheme (Jörg-Hess et al., 2014). The corrections at each grid point are a weighted average of all stations within a 35 km radius, weighted by the three-dimensional distance to the station location, whereby the vertical distance is scaled by a factor $\gamma = 50$ relative to the horizontal distance (following Oberrauch et al., 2024, Section 2.4.3). The gridded corrections obtained from the spatial interpolation are then applied to the downscaled gridded meteorological input data, forcing the distributed simulations.

The assimilation scheme notably improves snowpack simulations at unobserved locations across the domain at subregional scales, whereby its performance is ultimately constrained by the information content of the assimilated observations (Oberrauch et al., 2025). As a result, input datasets of varying quality and processing levels from the COSMO and ICON forecasting systems can be effectively corrected, yielding snowpack simulations of comparable accuracy regardless of the input data. This homogenization of the meteorological forcing ensures consistent quality of the provided dataset throughout the entire 10-year period, preventing year-to-year discontinuities, which may arise when switching NWP models (between COSMO and ICON) or processing levels (between forecast and analysis). A detailed evaluation of the assimilation scheme, comparing multiple assimilation settings over two seasons and a range of model complexities and input data qualities, is provided in Oberrauch et al. (2025).

3 Evaluation and Limitations

The OSHD model system has been successfully employed in an operational context for over a decade, delivering daily analyses and forecasts of snow cover dynamics across Switzerland, thereby providing critical information to the avalanche warning service, the Federal Office for the Environment, and other partners (Mott et al., 2023). In addition to its operational use, which relies on the system's robustness and the consistent quality of the data products delivered, continuous tuning, validation, and integration of advances from snow modeling research further contribute to the high quality of the data provided.

A recent validation study by Cluzet et al. (2024) compared snow wetness and snow cover fraction observations from Sentinel-1 and Sentinel-2 retrievals, respectively, against a pre-operational version of FSM2OSHD over five winter seasons from 2017 to 2021. They identified a delayed melt onset, particularly in southern aspects. Refining the albedo parameterization improved the modeled melt patterns, thereby substantially reducing biases in both the wet-snow line and the snow line of the model instance used here.

The representation of snow-canopy and canopy-atmosphere interactions within FSM2OSHD has been extensively validated at a process-level and for hyper-resolution simulations between 1 and 50 m (Mazzotti et al., 2020b, 2021, 2023). At the presented 250 m resolution, a comparison against PlanetScope RGB composites showed that FSM2OSHD accurately reproduces the observed differences in seasonal, interannual, and regional evolutions of the snowpack between open, densely, and sparsely forested areas (Haagmans et al., 2025).

https://doi.org/10.5194/egusphere-2026-159
Preprint. Discussion started: 2 February 2026

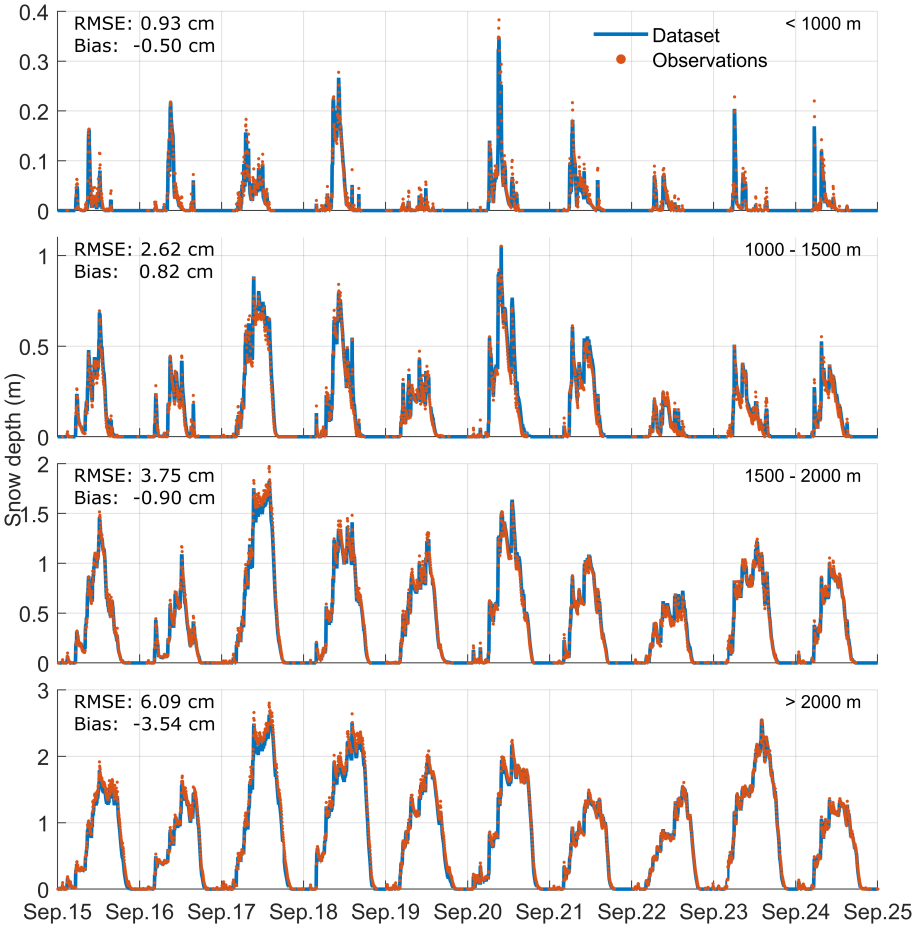

Figure 4. Simulated (blue line) and observed (orange dots) snow depth at 444 station locations between September 2015 and August 2025. Values are averaged over all stations within each elevation band. RMSE and bias are calculated over the entire period for all snow-covered days within the respective elevation bands (i.e., excluding days when both simulated and observed values are zero).

To provide an estimate of the uncertainties in the presented data, we compare snow depth estimates to 444 point observations covering the entire simulation period from September 2016 to September 2025. Average snow depths shown in Figure 4, aggregated into four distinct elevation bands, exhibit RMSE and bias values on the order of only a few centimeters. Even in the highest elevation band, with peak snow depths exceeding 2 m, the RMSE remains as low as 6 cm, with a slightly negative bias of 4 cm. It should be noted that these point observations are used during the assimilation step and are therefore not entirely independent. However, since the locally inferred corrections are interpolated in space, the presented validation against station data can be assumed to represent dataset errors at the targeted sub-regional scale. For a more in-depth validation of the assimilation scheme, please refer to (Oberrauch et al., 2024).

https://doi.org/10.5194/egusphere-2026-159
Preprint. Discussion started: 2 February 2026

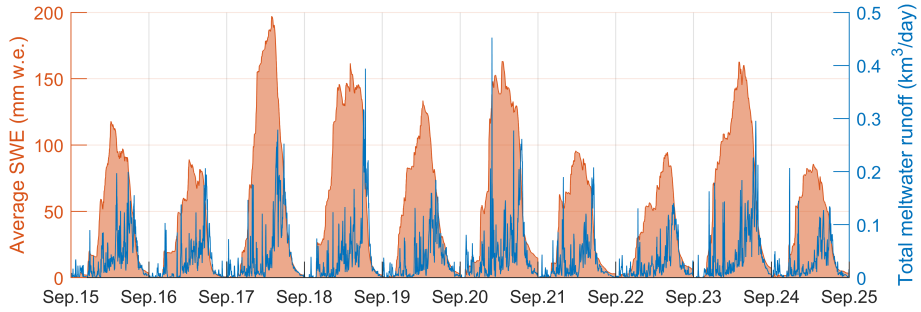

Figure 5. Daily time series of average SWE (orange shading, left axis) and total meltwater runoff (blue line, right axis) over the whole domain from September 2015 to August 2025.

The research model variant FSM2trans (Quéno et al., 2024) includes dedicated modules for snow redistribution by gravity- and wind-driven processes (Bernhardt and Schulz, 2010; Liston et al., 2007), as well as an updated density-dependent layering scheme to represent erodible snow. While accounting for horizontal redistribution of snow enables a more realistic representation of small-scale accumulation and erosion patterns, it requires simulations at hectometre or finer spatial resolutions, along with appropriate downscaling of wind fields (Quéno et al., 2024; Berg et al., 2024; Reynolds et al., 2024). At the resolution of 250 m of the presented dataset, FSM2OSHD does not explicitly account for snow redistribution, which may affect the accuracy of local-scale snow distribution patterns.

Snowpack estimates may be less reliable at very high elevations above 3 000 m a.s.l., where uncertainties are difficult to quantify due to the lack of comprehensive observational data. Moreover, a limited number of the highest grid cells are located outside the range of influence of any snow monitoring station. Hence, the assimilation scheme cannot infer any forcing corrections, and the input corresponds to the raw downscaled and bias-corrected NWP data.

4 Example usage

The presented dataset provides daily values of snow depth, SWE, SCF, and meltwater runoff over an area of 58 000 km^2 and a period of 10 years, enabling analyses across different temporal and spatial scales. Below, we highlight several illustrative examples of its use.

Figure 5 shows time series of the average SWE (orange shading, left axis) and total meltwater runoff over the entire domain (blue line, right axis). Over all 10 seasons, average peak-SWE amounts to 130 mm w.e., with around 90 mm w.e. for low-snow years and above 160 mm w.e. for high-snow years. Interannual variations in peak-SWE values are even more pronounced, ranging from up to 197 mm w.e. in water year 2018 down to 85 mm w.e. in water year 2025. While the overall seasonality is consistent, the magnitude of seasonal accumulation and melt varies notably. On average, peak-SWE typically occurs on March 24±18 days, but can be as early as the end of February and as late as the beginning of May (corresponding to a range of 65 days). Meltwater runoff also follows a clear seasonal pattern, with low values in autumn and winter, peak values in spring, and

https://doi.org/10.5194/egusphere-2026-159
Preprint. Discussion started: 2 February 2026

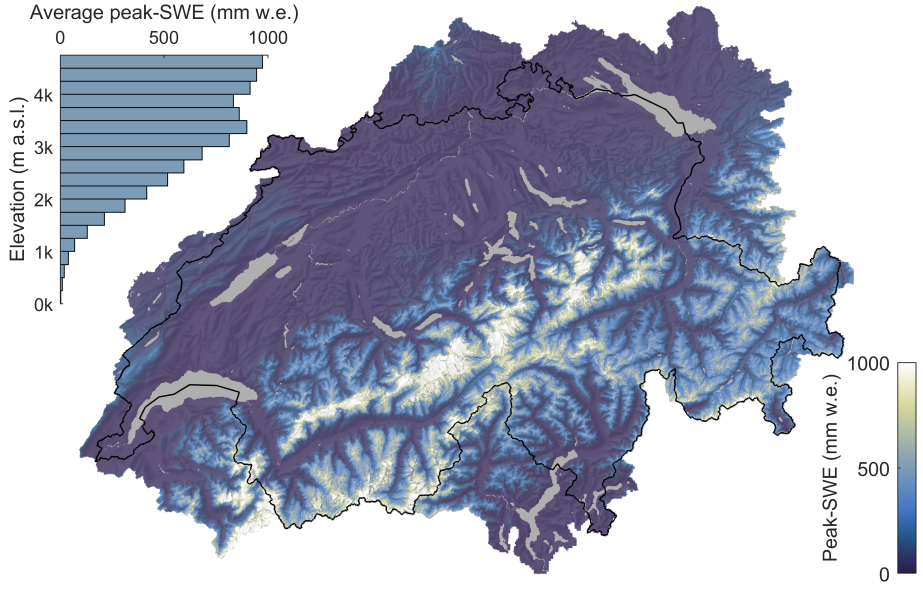

Figure 6. Map of average pixel-wise peak SWE between September 2015 and August 2025. The Swiss national border is outlined in black, and a shaded relief is used as background map.

a gradual reduction during summer. Day-to-day variability is, however, much higher, with pronounced spikes throughout the season and maximum values occurring as early as December (see water year 2021).

The average pixel-wise peak SWE over all 10 seasons, shown in Figure 6, reveals a distinct elevation-dependent pattern. In the high mountains and glaciated areas along the Alpine Main Ridge, peak SWE values regularly exceed 1 000 mm w.e. and even surpass 2 000 mm w.e.. In the mid-elevation mountain ranges between 2 000 m and 3 000 m a.s.l., average peak SWE is approximately 550 mm w.e.. Over the Swiss Plateau, the snowpack remains shallow, with considerably higher peak-SWE values observable in the adjacent Jura Mountains.

Figure 7 shows the snow melt-out date for each season, defined as the last day of the water year with at least 5 cm of snow cover, following a minimum of 30 consecutive days of snow cover. The Swiss Plateau rarely experiences a whole month of continuous snow cover, so a melt-out date cannot be computed for most of the region. In the Jura and Alpine foothills, the melt-out date typically falls between December and March, while snow cover can be observed up to June and later along the Main Alpine Ridge. Nevertheless, the interannual variability is considerable and total domain-wide SWE (shown in Figure 5) and melt-out dates are not necessarily correlated: in the low-snow year 2016, for instance, the average peak SWE was only 120 mm w.e., yet melt-out dates above 2 000 m ranged from June to September.

Figure 8 shows maps of the number of snow days per season (defined as days with a minimum snow depth of 5 cm) grouped into discrete classes between 1, 15, 30, 60, 120, and more than 365 days. Across all 10 years, much of the Swiss Alps exhibits a persistent seasonal snowpack with more than 120 snow days, while the Alpine foothills, Jura Mountains, and Swiss Plateau generally experience far fewer snow days. The water year 2020 shows a particularly distinct bimodal pattern, with areas

https://doi.org/10.5194/egusphere-2026-159
Preprint. Discussion started: 2 February 2026

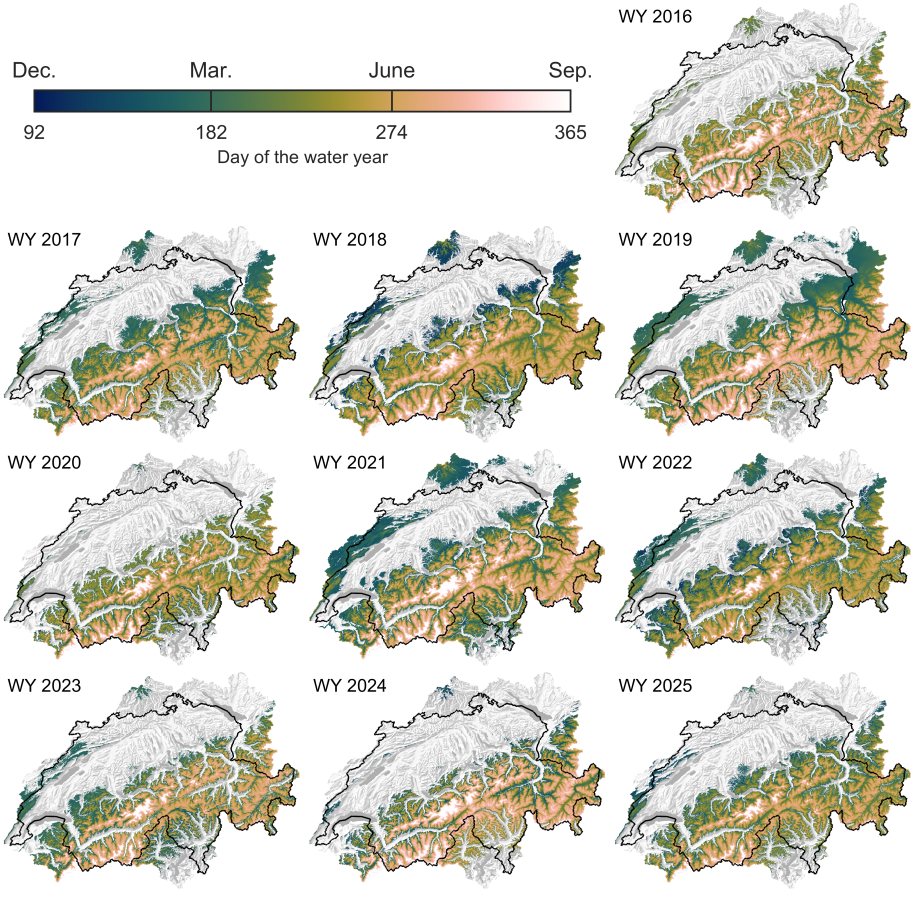

Figure 7. Maps of snow melt-out date for the water years 2016–2025. The snow melt-out date is defined as the last day of the water year with at least 5 cm of snow depth, following a minimum of 30 consecutive days of continuous snow cover. The Swiss national border is outlined in black, and a shaded relief is used as background map.

290 experiencing either more than 120 snow days or fewer than 15, and only narrow transition zones in between. The interannual variability is pronounced, not only between low and high elevations but also between the northern and southern slopes of the Alps. In most years, at least one day of snow cover occurs across the majority of the domain, although some exceptionally warm and/or dry years (e.g., 2020, 2022, and 2023) show snow-free conditions in the lowlands. Regions with 120 or more snow days and a snow cover that persists until the end of the season (labeled as > 365 in the figure) are confined to small areas
295 in the highest and glaciated parts of the Alps and are virtually absent in certain years, such as 2017.

https://doi.org/10.5194/egusphere-2026-159
Preprint. Discussion started: 2 February 2026

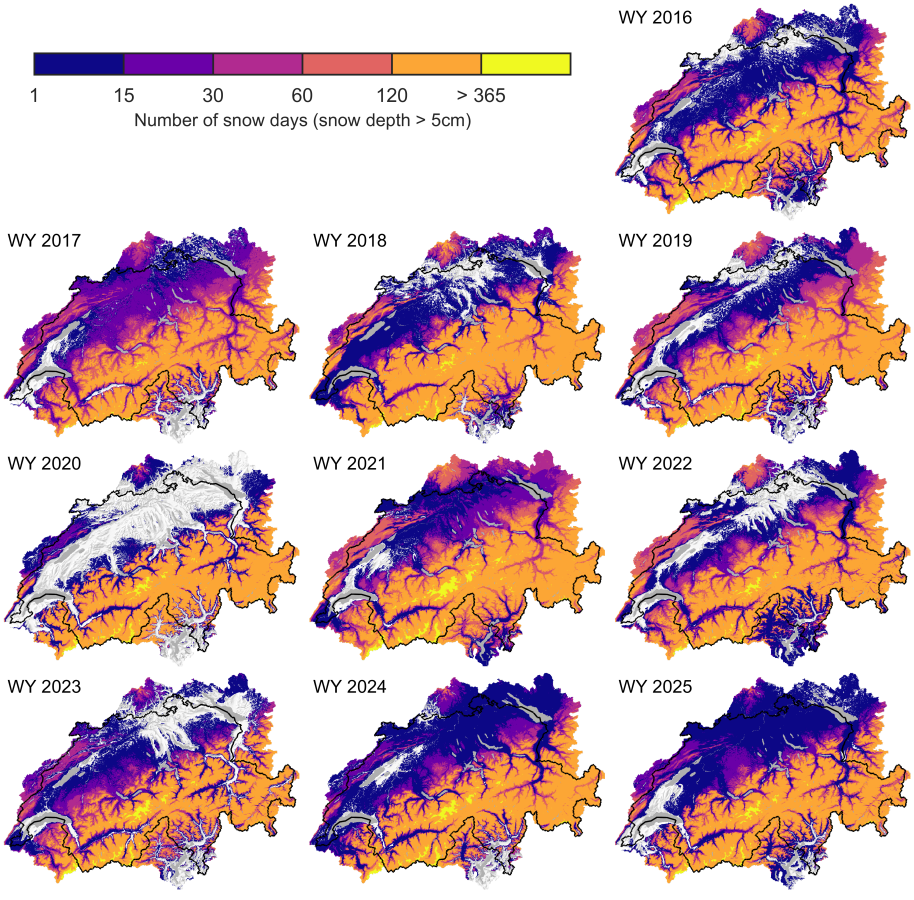

Figure 8. Maps of the number of snow days per season (defined as days with a minimum snow depth of 5 cm) for water years 2016 to 2025. Regions with 120 or more snow days and a snow cover that persists until the end of the season are labeled as >365. The Swiss national border is outlined in black, and a shaded relief is used as background map.

5 Data format

The dataset provides daily estimates of snow depth (m), snow water equivalent (mm w.e. ≡ kg m^{-2}), snow cover fraction (unitless), and snowmelt runoff (mm day^{-1} ≡ kg m^{-2} day^{-1}) for each grid cell within the domain. The reference time for daily values is 06:00 Central European Time (CET ≡ UTC+01:00), with snow depth, SWE, and SCF representing states at that time, and runoff corresponding to the accumulated total over the preceding 24 hours. Given that on September 1 at 6:00 CET of each season, all snow is removed, all variables for that day in the dataset are zero because the end-states from the previous season are not carried over.

The data are stored in self-explanatory monthly NetCDF files (e.g., `OSHD_DATA_2020-01.nc` for January 2020) within individual zip archives for each water year (e.g., `OSHD_DATA_WY2020.zip` for water year 2020). Variable names, attributes, and metadata adhere to the CF 1.12 and ACDD 1.3 conventions. The data variables are structured as three-dimensional ar-

https://doi.org/10.5194/egusphere-2026-159
Preprint. Discussion started: 2 February 2026

rays, with time, easting, and northing coordinates. The temporal coordinate denotes the number of days since the first day of the corresponding month. The horizontal coordinates refer to the center of the respective grid cell, given in the local Swiss CH1903+/LV95 reference system (EPSG: 2056). The total spatial extent is also specified by the minimum and maximum longitude and latitude in WGS84 coordinates (EPSG:4326). Additional metadata contains title, keywords, summary, contact information, and version history. The model DEM is provided as a GeoTiff (`OSHD_MODEL_DEM.tif`). Compatibility with the NASA Panoply NetCDF Viewer (NASA GISS, 2025) was verified using Panoply v5.7.1 under Windows 11.

6 Conclusions

We present a reanalysis dataset of spatially explicit seasonal snow cover dynamics for Switzerland and its bordering regions for water years 2016 to 2025, based on the high-resolution simulations with the physics-based, multi-layer snow model FSM2OSHD and the assimilation of snow depth observations from 444 stations across the domain. The combination of dedicated downscaling of NWP forcing data with the upscaling of state-of-the-art hyper-resolution DEM and light-availability datasets enables simulations that account for subgrid variability within the 250 m model resolution, which is crucial for capturing the spatial heterogeneity of the mountainous snowpack. The coupled energy- and mass-balance equation, solved for individual numerical snow layers, explicitly accounts for different atmospheric and snowpack processes of open, forested, and glaciated areas. Finally, the assimilation of in situ snow depth observations dynamically corrects spatiotemporal error patterns in the meteorological input data, ensuring consistent forcing quality over the presented 10-year period.

Spanning 10 years of physically consistent snow cover estimates across a large part of the European Alps, the dataset contributes to the snow data record for a region characterized by complex terrain and diverse hydroclimatic regimes. With its high spatial and temporal resolution, the dataset helps bridge the gap between coarse global products and detailed local observations. The data are publicly and freely available at https://zenodo.org/records/17313889?preview=1&token=eyJhbGciOiJIUzUxMiJ9.eyJpZCI6IjhkOTgwNDcyLWI3ZWYtNGZmOS1iY2VkLTFjZTkyMmNmMzFhZCIsImRhdGEiOnt9LCJyYW5kb20iOiI2ZTEwZjVhZDdmNGZlZWE2NjIyYjBlMzkzM2M2NGFmMyJ9.cu88BUCkEuh0UH37WTvSZTIbDiqw331U6yF7T51TbhQMUvOv4pmmrA2bN2LEs6NJhW1Pp4Zdm7BTqNUvU0O7Lw (Oberrauch et al., 2026), providing a robust foundation for hydrological, ecological, and cryospheric analyses.

Data availability. The dataset is publicly available at https://zenodo.org/records/17313889?preview=1&token=eyJhbGciOiJIUzUxMiJ9.eyJpZCI6IjhkOTgwNDcyLWI3ZWYtNGZmOS1iY2VkLTFjZTkyMmNmMzFhZCIsImRhdGEiOnt9LCJyYW5kb20iOiI2ZTEwZjVhZDdmNGZlZWE2NjIyYjBlMzkzM2M2NGFmMyJ9.cu88BUCkEuh0UH37WTvSZTIbDiqw331U6yF7T51TbhQMUvOv4pmmrA2bN2LEs6NJhW1Pp4Zdm7BTqNUvU0O7Lw (Oberrauch et al., 2026) under a CC BY 4.0 license, permitting use, adaptation, and redistribution with appropriate attribution to the creators and the original dataset. Data are compressed into self-explanatory zip archives for each water year (e.g., `OSHD_DATA_WY2020.zip` for water year 2020), containing monthly NetCDF files (e.g., `OSHD_DATA_2020-01.nc` for January 2020) with all relevant metadata conforming to the CF 1.12 and ACDD 1.3 conventions. The model digital elevation model (DEM)

https://doi.org/10.5194/egusphere-2026-159
Preprint. Discussion started: 2 February 2026

is distributed as a GeoTIFF file named `OSHD_MODEL_DEM.tif`. Sources of all input datasets and model codes used in this study are detailed in the accompanying publication.

Author contributions. MO performed the simulations, conducted the analysis, produced the figures, compiled the final dataset, and wrote the manuscript, all under the supervision of TJ. BC, JM, GM, RM, LQ, CW, and TJ contributed to the model development. GM, CW, and TJ processed forest and light availability data. BC, JM, RM, LQ, TZ, and TJ curated the input, land cover, and observational datasets. MO, BC, and JM implemented the assimilation scheme. All authors contributed to the analysis, supported the writing of the manuscript, and reviewed and approved the final version.

Competing interests. The authors declare that they have no competing interests.

Acknowledgements. This work forms part of the Swiss National Science Foundation–funded project “Improved methods for incorporating observational data into physics-based, multi-layer snow models” (grant No. 192140, https://data.snf.ch/grants/grant/192140). Parts of the text were refined with the assistance of generative AI to improve clarity and readability, subsequently reviewed and verified by the authors.

https://doi.org/10.5194/egusphere-2026-159
Preprint. Discussion started: 2 February 2026

References

Alonso-González, E., Ignacio López-Moreno, J., Gascoin, S., García-Valdecasas Ojeda, M., Sanmiguel-Vallelado, A., Navarro-Serrano, F., Revuelto, J., Ceballos, A., Jesús, M., Parra, E., and Essery, R.: Daily gridded datasets of snow depth and snow water equivalent for the Iberian Peninsula from 1980 to 2014, Earth Syst. Sci. Data, 10, 303–315, https://doi.org/10.5194/essd-10-303-2018, 2018.

Alonso-González, E., Aalstad, K., Pirk, N., Mazzolini, M., Treichler, D., Leclercq, P., Westermann, S., López-Moreno, J. I., and Gascoin, S.: Spatio-temporal information propagation using sparse observations in hyper-resolution ensemble-based snow data assimilation, Hydrol. Earth Syst. Sci, 27, 4637–4659, https://doi.org/10.5194/hess-27-4637-2023, 2023.

Anderson, E. A.: A Point Energy and Mass Balance Model of a Snow Cover, Tech. rep., National Oceanic and Atmospheric Administration (NOAA), U.S. Department of Commerce, https://repository.library.noaa.gov/view/noaa/6392/noaa_6392_DS1.pdf, 1976.

Avanzi, F., Gabellani, S., Delogu, F., Silvestro, F., Pignone, F., Bruno, G., Pulvirenti, L., Squicciarino, G., Fiori, E., Rossi, L., Puca, S., Toniazzo, A., Giordano, P., Falzacappa, M., Ratto, S., Stevenin, H., Cardillo, A., Fioletti, M., Cazzuli, O., Cremonese, E., Morra Di Cella, U., and Ferraris, L.: IT-SNOW: a snow reanalysis for Italy blending modeling, in situ data, and satellite observations (2010-2021), Earth Syst. Sci. Data, 15, 639–660, https://doi.org/10.5194/essd-15-639-2023, 2023.

Baldauf, M., Seifert, A., Förstner, J., Majewski, D., Raschendorfer, M., and Reinhardt, T.: Operational Convective-Scale Numerical Weather Prediction with the COSMO Model: Description and Sensitivities, Monthly Weather Review, 139, 3887–3905, https://doi.org/10.1175/MWR-D-10-05013.1, 2011.

Barrett, A. P.: National Operational Hydrologic Remote Sensing Center SNOw Data Assimilation System (SNODAS) Products at NSIDC - NSIDC Special Report 11, Tech. Rep. NSIDC Special Report 11, National Snow and Ice Data Center, Boulder, Colorado, USA, 2003.

Berg, J., Reynolds, D., Quéno, L., Jonas, T., Lehning, M., and Mott, R.: A seasonal snowpack model forced with dynamically downscaled forcing data resolves hydrologically relevant accumulation patterns, Frontiers in Earth Science, 12, 1393 260, https://doi.org/10.3389/feart.2024.1393260, 2024.

Bernhardt, M. and Schulz, K.: SnowSlide: A simple routine for calculating gravitational snow transport, Geophysical Research Letters, 37, 11 502, https://doi.org/10.1029/2010GL043086, 2010.

Boone, A. and Etchevers, P.: An Intercomparison of Three Snow Schemes of Varying Complexity Coupled to the Same Land Surface Model: Local-Scale Evaluation at an Alpine Site, Journal of Hydrometeorology, 2, 374–394, https://doi.org/10.1175/1525-7541(2001)002<0374:AIOTSS>2.0.CO;2, 2001.

Bühle, L. J., Marty, M., Eberhard, L. A., Stoffel, A., Hafner, E. D., and Bühler, Y.: Spatially continuous snow depth mapping by aeroplane photogrammetry for annual peak of winter from 2017 to 2021 in open areas, The Cryosphere, 17, 3383–3408, https://doi.org/10.5194/tc-17-3383-2023, 2023.

Chopin, N. and Papaspiliopoulos, O.: An Introduction to Sequential Monte Carlo, vol. 4 of *Springer Series in Statistics*, Springer International Publishing, Cham, ISBN 978-3-030-47844-5, https://doi.org/10.1007/978-3-030-47845-2, 2020.

Cluzet, B., Magnusson, J., Quéno, L., Mazzotti, G., Mott, R., and Jonas, T.: Exploring how Sentinel-1 wet-snow maps can inform fully distributed physically based snowpack models, The Cryosphere, 18, 5753–5767, https://doi.org/10.5194/tc-18-5753-2024, 2024.

Cox, P. M., Betts, R. A., Bunton, C. B., Essery, R. L. H., Rowntree, P. R., and Smith, J.: The impact of new land surface physics on the GCM simulation of climate and climate sensitivity, Climate Dynamics, 15, 183–203, https://doi.org/10.1007/s003820050276, 1999.

Douville, H., Royer, J. F., and Mahfouf, J. F.: A new snow parameterization for the Météo-France climate model: Part I: validation in stand-alone experiments, Climate Dynamics, 12, 21–35, https://doi.org/10.1007/BF00208760, 1995.

https://doi.org/10.5194/egusphere-2026-159
Preprint. Discussion started: 2 February 2026

Dozier, J., Bair, E. H., and Davis, R. E.: Estimating the spatial distribution of snow water equivalent in the world's mountains, WIREs Water, 3, 461–474, https://doi.org/10.1002/wat2.1140, 2016.

Eckert, N., Corona, C., Giacona, F., Gaume, J., Mayer, S., van Herwijnen, A., Hagenmuller, P., and Stoffel, M.: Climate change impacts on snow avalanche activity and related risks, Nature Reviews Earth & Environment, 5, 369–389, https://doi.org/10.1038/s43017-024-00540-2, 2024.

Essery, R.: A factorial snowpack model (FSM 1.0), Geoscientific Model Development, 8, 3867–3876, https://doi.org/10.5194/gmd-8-3867-2015, 2015.

Essery, R., Mazzotti, G., Barr, S., Jonas, T., Quaife, T., and Rutter, N.: A Flexible Snow Model (FSM 2.1.1) including a forest canopy, Geoscientific Model Development, 18, 3583–3605, https://doi.org/10.5194/gmd-18-3583-2025, 2025.

European Union's Copernicus Land Monitoring Service information: CORINE Land Cover 2018 (vector/raster 100 m), Europe, 6-yearly, https://doi.org/10.2909/960998c1-1870-4e82-8051-6485205ebbac, 2020.

Fang, Y., Liu, Y., and Margulis, S. A.: A western United States snow reanalysis dataset over the Landsat era from water years 1985 to 2021, Scientific Data, 9, 1–17, https://doi.org/10.1038/S41597-022-01768-7, 2022.

Fiddes, J., Aalstad, K., and Westermann, S.: Hyper-resolution ensemble-based snow reanalysis in mountain regions using clustering, Hydrology and Earth System Sciences, 23, 4717–4736, https://doi.org/10.5194/HESS-23-4717-2019, 2019.

Floriancic, M. G., Berghuijs, W. R., Jonas, T., Kirchner, J. W., and Molnar, P.: Effects of climate anomalies on warm-season low flows in Switzerland, Hydrology and Earth System Sciences, 24, 5423–5438, https://doi.org/10.5194/HESS-24-5423-2020, 2020.

Gascoin, S., Grizonnet, M., Bouchet, M., Salgues, G., and Hagolle, O.: Theia Snow collection: High-resolution operational snow cover maps from Sentinel-2 and Landsat-8 data, Earth System Science Data, 11, 493–514, https://doi.org/10.5194/ESSD-11-493-2019, 2019.

Gascoin, S., Luojus, K., Nagler, T., Lievens, H., Masiokas, M., Jonas, T., Zheng, Z., and De Rosnay, P.: Remote sensing of mountain snow from space: status and recommendations, Frontiers in Earth Science, 12, 1381 323, https://doi.org/10.3389/feart.2024.1381323, 2024.

Griessinger, N., Seibert, J., Magnusson, J., and Jonas, T.: Assessing the benefit of snow data assimilation for runoff modeling in Alpine catchments, Hydrol. Earth Syst. Sci, 20, 3895–3905, https://doi.org/10.5194/hess-20-3895-2016, 2016.

Grünewald, T., Schirmer, M., Mott, R., and Lehning, M.: Spatial and temporal variability of snow depth and ablation rates in a small mountain catchment, The Cryosphere, 4, 215–225, https://doi.org/10.5194/TC-4-215-2010, 2010.

Gubler, S., Fukutome, S., and Scherrer, S. C.: On the statistical distribution of temperature and the classification of extreme events considering season and climate change—an application in Switzerland, Theoretical and Applied Climatology, 153, 1273–1291, https://doi.org/10.1007/s00704-023-04530-0, 2023.

Günther, D., Marke, T., Essery, R., and Strasser, U.: Uncertainties in Snowpack Simulations—Assessing the Impact of Model Structure, Parameter Choice, and Forcing Data Error on Point-Scale Energy Balance Snow Model Performance, Water Resources Research, 55, 2779–2800, https://doi.org/10.1029/2018WR023403, 2019.

Haagmans, V., Mazzotti, G., Webster, C., and Jonas, T.: How montane forests shape snow cover dynamics across the central European Alps, https://doi.org/10.5194/egusphere-2025-3843, 2025.

Hale, K. E., Musselman, K. N., Newman, A. J., Livneh, B., and Molotch, N. P.: Effects of Snow Water Storage on Hydrologic Partitioning Across the Mountainous, Western United States, Water Resources Research, 59, e2023WR034 690, https://doi.org/10.1029/2023WR034690, 2023.

Han, J., Liu, Z., Woods, R., McVicar, T. R., Yang, D., Wang, T., Hou, Y., Guo, Y., Li, C., and Yang, Y.: Streamflow seasonality in a snow-dwindling world, Nature, 629, 1075–1081, https://doi.org/10.1038/s41586-024-07299-y, 2024.

https://doi.org/10.5194/egusphere-2026-159
Preprint. Discussion started: 2 February 2026

Helbig, N., Schirmer, M., Magnusson, J., Mäder, F., van Herwijnen, A., Quéno, L., Bühler, Y., Deems, J. S., and Gascoin, S.: A seasonal algorithm of the snow-covered area fraction for mountainous terrain, The Cryosphere, 15, 4607–4624, https://doi.org/10.5194/tc-15-4607-2021, 2021.

Hersbach, H., Bell, B., Berrisford, P., Hirahara, S., Horányi, A., Muñoz-Sabater, J., Nicolas, J., Peubey, C., Radu, R., Schepers, D., Simmons, A., Soci, C., Abdalla, S., Abellan, X., Balsamo, G., Bechtold, P., Biavati, G., Bidlot, J., Bonavita, M., De Chiara, G., Dahlgren, P., Dee, D., Diamantakis, M., Dragani, R., Flemming, J., Forbes, R., Fuentes, M., Geer, A., Haimberger, L., Healy, S., Hogan, R. J., Hólm, E., Janisková, M., Keeley, S., Laloyaux, P., Lopez, P., Lupu, C., Radnoti, G., de Rosnay, P., Rozum, I., Vamborg, F., Villaume, S., and Thépaut, J. N.: The ERA5 global reanalysis, Quarterly Journal of the Royal Meteorological Society, 146, 1999–2049, https://doi.org/10.1002/QJ.3803, 2020.

Hou, Y., Yang, Y., Han, J., Woods, R., and Yan, Z.: Impacts of snow changes on hydropower potential under a changing climate, Journal of Hydrology, 661, 133 747, https://doi.org/10.1016/J.JHYDROL.2025.133747, 2025.

Jenicek, M., Seibert, J., Zappa, M., Staudinger, M., and Jonas, T.: Importance of maximum snow accumulation for summer low flows in humid catchments, Hydrology and Earth System Sciences, 20, 859–874, https://doi.org/10.5194/hess-20-859-2016, 2016.

Jonas, T., Webster, C., Mazzotti, G., and Malle, J.: HPEval: A canopy shortwave radiation transmission model using high-resolution hemispherical images, Agricultural and Forest Meteorology, 284, 107 903, https://doi.org/10.1016/J.AGRFORMET.2020.107903, 2020.

Jörg-Hess, S., Fundel, F., Jonas, T., and Zappa, M.: The Cryosphere Homogenisation of a gridded snow water equivalent climatology for Alpine terrain: methodology and applications, The Cryosphere, 8, 471–485, https://doi.org/10.5194/tc-8-471-2014, 2014.

Kavetski, D. and Kuczera, G.: Model smoothing strategies to remove microscale discontinuities and spurious secondary optima in objective functions in hydrological calibration, Water Resources Research, 43, 3411, https://doi.org/10.1029/2006WR005195, 2007.

Kouki, K., Luojus, K., and Riihelä, A.: Evaluation of snow cover properties in ERA5 and ERA5-Land with several satellite-based datasets in the Northern Hemisphere in spring 1982-2018, Cryosphere, 17, 5007–5026, https://doi.org/10.5194/TC-17-5007-2023, 2023.

Largeron, C., Dumont, M., Morin, S., Boone, A., Lafaysse, M., Metref, S., Cosme, E., Jonas, T., Winstral, A., and Margulis, S. A.: Toward Snow Cover Estimation in Mountainous Areas Using Modern Data Assimilation Methods: A Review, Frontiers in Earth Science, 8, https://doi.org/10.3389/feart.2020.00325, 2020.

Li, D., Lettenmaier, D. P., Margulis, S. A., and Andreadis, K.: The Role of Rain-on-Snow in Flooding Over the Conterminous United States, Water Resources Research, 55, 8492–8513, https://doi.org/10.1029/2019WR024950, 2019.

Li, W., Chen, J., Li, L., Orsolini, Y. J., Xiang, Y., Senan, R., and De Rosnay, P.: Impacts of snow assimilation on seasonal snow and meteorological forecasts for the Tibetan Plateau, Cryosphere, 16, 4985–5000, https://doi.org/10.5194/TC-16-4985-2022,, 2022.

Lievens, H., Demuzere, M., Marshall, H.-P., Reichle, R. H., Brucker, L., Brangers, I., de Rosnay, P., Dumont, M., Girotto, M., Immerzeel, W. W., Jonas, T., Kim, E. J., Koch, I., Marty, C., Saloranta, T., Schöber, J., and De Lannoy, G. J. M.: Snow depth variability in the Northern Hemisphere mountains observed from space, Nature Communications, 10, 4629, https://doi.org/10.1038/s41467-019-12566-y, 2019.

Lievens, H., Brangers, I., Marshall, H.-P., Jonas, T., Olefs, M., and De Lannoy, G.: Sentinel-1 snow depth retrieval at sub-kilometer resolution over the European Alps, The Cryosphere, 16, 159–177, https://doi.org/10.5194/tc-16-159-2022, 2022.

Liston, G. E., Haehnel, R. B., Sturm, M., Hiemstra, C. A., Berezovskaya, S., and Tabler, R. D.: Simulating complex snow distributions in windy environments using SnowTran-3D, Journal of Glaciology, 53, 241–256, https://doi.org/10.3189/172756507782202865, 2007.

Liu, Y., Fang, Y., and Margulis, S. A.: Spatiotemporal distribution of seasonal snow water equivalent in High Mountain Asia from an 18-year Landsat-MODIS era snow reanalysis dataset, Cryosphere, 15, 5261–5280, https://doi.org/10.5194/TC-15-5261-2021, 2021.

https://doi.org/10.5194/egusphere-2026-159
Preprint. Discussion started: 2 February 2026

López-Moreno, J. I., Fassnacht, S. R., Heath, J. T., Musselman, K. N., Revuelto, J., Latron, J., Morán-Tejeda, E., and Jonas, T.: Small scale spatial variability of snow density and depth over complex alpine terrain: Implications for estimating snow water equivalent, Advances in Water Resources, 55, 40–52, https://doi.org/10.1016/J.ADVWATRES.2012.08.010, 2013.

Louis, J.-F.: A parametric model of vertical eddy fluxes in the atmosphere, Boundary-Layer Meteorology, 17, 187–202, https://doi.org/10.1007/BF00117978, 1979.

Magnusson, J., Gustafsson, D., Hüsler, F., and Jonas, T.: Assimilation of point SWE data into a distributed snow cover model comparing two contrasting methods, Water Resources Research, 50, 7816–7835, https://doi.org/10.1002/2014WR015302, 2014.

Magnusson, J., Nævdal, G., Matt, F., Burkhart, J. F., and Winstral, A.: Improving hydropower inflow forecasts by assimilating snow data, Hydrology Research, 51, 226–237, https://doi.org/10.2166/NH.2020.025, 2020.

Magnusson, J., Bühler, Y., Quéno, L., Cluzet, B., Mazzotti, G., Webster, C., Mott, R., and Jonas, T.: High-resolution hydrometeorological and snow data for the Dischma catchment in Switzerland, Earth System Science Data, 17, 703–717, https://doi.org/10.5194/essd-17-703-2025, 2025.

Margulis, S. A., Cortés, G., Girotto, M., and Durand, M.: A Landsat-Era Sierra Nevada Snow Reanalysis (1985–2015), Journal of Hydrometeorology, 17, 1203–1221, https://doi.org/10.1175/JHM-D-15-0177.1, 2016.

Mazzotti, G., Essery, R., Moeser, C. D., and Jonas, T.: Resolving Small-Scale Forest Snow Patterns Using an Energy Balance Snow Model With a One-Layer Canopy, Water Resources Research, 56, https://doi.org/10.1029/2019WR026129, 2020a.

Mazzotti, G., Essery, R., Webster, C., Malle, J., and Jonas, T.: Process-Level Evaluation of a Hyper-Resolution Forest Snow Model Using Distributed Multisensor Observations, Water Resources Research, 56, https://doi.org/10.1029/2020WR027572, 2020b.

Mazzotti, G., Webster, C., Essery, R., and Jonas, T.: Increasing the Physical Representation of Forest-Snow Processes in Coarse-Resolution Models: Lessons Learned From Upscaling Hyper-Resolution Simulations, Water Resources Research, 57, e2020WR029 064, https://doi.org/10.1029/2020WR029064, 2021.

Mazzotti, G., Webster, C., Quéno, L., Cluzet, B., and Jonas, T.: Canopy structure, topography, and weather are equally important drivers of small-scale snow cover dynamics in sub-alpine forests, Hydrology and Earth System Sciences, 27, 2099–2121, https://doi.org/10.5194/hess-27-2099-2023, 2023.

Menard, C. B., Essery, R., Krinner, G., Arduini, G., Bartlett, P., Boone, A., Brutel-Vuilmet, C., Burke, E., Cuntz, M., Dai, Y., Decharme, B., Dutra, E., Fang, X., Fierz, C., Gusev, Y., Hagemann, S., Haverd, V., Kim, H., Lafaysse, M., Marke, T., Nasonova, O., Nitta, T., Niwano, M., Pomeroy, J., Schädler, G., Semenov, V. A., Smirnova, T., Strasser, U., Swenson, S., Turkov, D., Wever, N., and Yuan, H.: Scientific and Human Errors in a Snow Model Intercomparison, Bulletin of the American Meteorological Society, 102, E61–E79, https://doi.org/10.1175/BAMS-D-19-0329.1, 2021.

MeteoSwiss: Project ICON-22 - MeteoSwiss, 2023.

MeteoSwiss: The introduction of the new weather model ICON marks a milestone in Swiss weather forecasting - MeteoSwiss, 2024.

MeteoSwiss: The climate of Switzerland - MeteoSwiss, https://www.meteoswiss.admin.ch/climate/the-climate-of-switzerland.html, 2025.

Monteiro, D. and Morin, S.: Multi-decadal analysis of past winter temperature, precipitation and snow cover data in the European Alps from reanalyses, climate models and observational datasets, Cryosphere, 17, 3617–3660, https://doi.org/10.5194/TC-17-3617-2023, 2023.

Moreno-Gené, J., Sánchez-Pulido, L., Cristobal-Fransi, E., and Daries, N.: The Economic Sustainability of Snow Tourism: The Case of Ski Resorts in Austria, France, and Italy, Sustainability 2018, Vol. 10, Page 3012, 10, 3012, https://doi.org/10.3390/SU10093012, 2018.

Morin, S., Samacoïts, R., François, H., Carmagnola, C. M., Abegg, B., Demiroglu, O. C., Pons, M., Soubeyroux, J. M., Lafaysse, M., Franklin, S., Griffiths, G., Kite, D., Hoppler, A. A., George, E., Buontempo, C., Almond, S., Dubois, G., and Cauchy,

https://doi.org/10.5194/egusphere-2026-159
Preprint. Discussion started: 2 February 2026

A.: Pan-European meteorological and snow indicators of climate change impact on ski tourism, Climate Services, 22, 100 215, https://doi.org/10.1016/J.CLISER.2021.100215, 2021.

Mortimer, C. and Vionnet, V.: Northern Hemisphere in situ snow water equivalent dataset (NorSWE, 1979–2021), Earth System Science Data, 17, 3619–3640, https://doi.org/10.5194/essd-17-3619-2025, 2025.

Mortimer, C., Mudryk, L., Derksen, C., Luojus, K., Brown, R., Kelly, R., and Tedesco, M.: Evaluation of long-term Northern Hemisphere snow water equivalent products, Cryosphere, 14, 1579–1594, https://doi.org/10.5194/TC-14-1579-2020, 2020.

Mott, R., Vionnet, V., and Grünewald, T.: The Seasonal Snow Cover Dynamics: Review on Wind-Driven Coupling Processes, Frontiers in Earth Science, 6, 197, https://doi.org/10.3389/feart.2018.00197, 2018.

Mott, R., Winstral, A., Cluzet, B., Helbig, N., Magnusson, J., Mazzotti, G., Quéno, L., Schirmer, M., Webster, C., and Jonas, T.: Operational snow-hydrological modeling for Switzerland, Frontiers in Earth Science, 11, https://doi.org/10.3389/feart.2023.1228158, 2023.

Musselman, K. N., Lehner, F., Ikeda, K., Clark, M. P., Prein, A. F., Liu, C., Barlage, M., and Rasmussen, R.: Projected increases and shifts in rain-on-snow flood risk over western North America, Nature Climate Change, 8, 808–812, https://doi.org/10.1038/s41558-018-0236-4, 2018.

Musselman, K. N., Addor, N., Vano, J. A., and Molotch, N. P.: Winter melt trends portend widespread declines in snow water resources, Nature Climate Change, 11, 418–424, https://doi.org/10.1038/S41558-021-01014-9, 2021.

NASA GISS: Panoply 5 netCDF, HDF and GRIB Data Viewer, https://www.giss.nasa.gov/tools/panoply/, 2025.

Oberrauch, M., Cluzet, B., Magnusson, J., and Jonas, T.: Improving Fully Distributed Snowpack Simulations by Mapping Perturbations of Meteorological Forcings Inferred From Particle Filter Assimilation of Snow Monitoring Data, Water Resources Research, 60, https://doi.org/10.1029/2023WR036994, 2024.

Oberrauch, M., Cluzet, B., Magnusson, J., and Jonas, T.: The Performance Gains of Assimilating Limited Information Into a Fully Distributed Snowpack Model Depend on Model Complexity and Input Data Quality, Water Resources Research, 61, https://doi.org/10.1029/2025WR040681, 2025.

Oberrauch, M., Cluzet, B., Magnusson, J., Mazzotti, G., Mott, R., Quéno, L., Webster, C., Zolles, T., and Jonas, T.: A high-resolution snow dataset for Switzerland (2016-2025) combining physics-based simulations and in situ observations, https://zenodo.org/records/17313889?preview=1&token=eyJhbGciOiJIUzUxMiJ9.eyJpZCI6IjhkOTgwNDcyLWI3ZWYtNGZmOS1iY2VkLTFjZTkyMmNmMzFhZCIsImRhdGEiOnt9LCJyYW5kb20iOiI2ZTEwZjVhZDdmNGZlZWE2NjIyYjBlMzkzM2M2NGFmMyJ9.cu88BUCkEuh0UH37WTvSZTIbDiqw331U6yF7T51TbhQMUvOv4pmmrA2bN2LEs6NJhW1Pp4Zdm7BTqNUvU0O7Lw, 2026.

Odry, J., Boucher, M.-A., Lachance-Cloutier, S., Turcotte, R., and St-Louis, P.-Y.: Large-scale snow data assimilation using a spatialized particle filter: recovering the spatial structure of the particles, The Cryosphere, 16, 3489–3506, https://doi.org/10.5194/tc-16-3489-2022, 2022.

Olefs, M., Koch, R., Schöner, W., and Marke, T.: Changes in Snow Depth, Snow Cover Duration, and Potential Snowmaking Conditions in Austria, 1961–2020—A Model Based Approach, Atmosphere 2020, Vol. 11, Page 1330, 11, 1330, https://doi.org/10.3390/ATMOS11121330, 2020.

Painter, T. H., Berisford, D. F., Boardman, J. W., Bormann, K. J., Deems, J. S., Gehrke, F., Hedrick, A., Joyce, M., Laidlaw, R., Marks, D., Mattmann, C., McGurk, B., Ramirez, P., Richardson, M., Skiles, S. M. K., Seidel, F. C., and Winstral, A.: The Airborne Snow Observatory: Fusion of scanning lidar, imaging spectrometer, and physically-based modeling for mapping snow water equivalent and snow albedo, Remote Sensing of Environment, 184, 139–152, https://doi.org/10.1016/j.rse.2016.06.018, 2016.

https://doi.org/10.5194/egusphere-2026-159
Preprint. Discussion started: 2 February 2026

Publications Office of the European Union: Drought in Europe – March 2023 – GDO analytical report, Tech. rep., https://doi.org/doi/10.2760/998985, 2023.

Quéno, L., Mott, R., Morin, P., Cluzet, B., Mazzotti, G., and Jonas, T.: Snow redistribution in an intermediate-complexity snow hydrology modelling framework, The Cryosphere, 18, 3533–3557, https://doi.org/10.5194/tc-18-3533-2024, 2024.

Rasul, G. and Molden, D.: The Global Social and Economic Consequences of Mountain Cryospheric Change, Frontiers in Environmental Science, 7, 91, https://doi.org/10.3389/fenvs.2019.00091, 2019.

Revuelto, J., Azorin-Molina, C., Alonso-González, E., Sanmiguel-Vallelado, A., Navarro-Serrano, F., Rico, I., and López-Moreno, J. I.: Meteorological and snow distribution data in the Izas Experimental Catchment (Spanish Pyrenees) from 2011 to 2017, Earth Syst. Sci. Data, 9, 993–1005, https://doi.org/10.5194/essd-9-993-2017, 2017.

Reynolds, D., Quéno, L., Lehning, M., Jafari, M., Berg, J., Jonas, T., Haugeneder, M., and Mott, R.: Seasonal snow-atmosphere modeling: let's do it, The Cryosphere, 18, 4315–4333, https://doi.org/10.5194/tc-18-4315-2024, 2024.

Siirila-Woodburn, E. R., Rhoades, A. M., Hatchett, B. J., Huning, L. S., Szinai, J., Tague, C., Nico, P. S., Feldman, D. R., Jones, A. D., Collins, W. D., and Kaatz, L.: A low-to-no snow future and its impacts on water resources in the western United States, Nature Reviews Earth & Environment, 2, 800–819, https://doi.org/10.1038/s43017-021-00219-y, 2021.

Slatyer, R. A., Umbers, K. D., and Arnold, P. A.: Ecological responses to variation in seasonal snow cover, Conservation Biology, 36, e13 727, https://doi.org/10.1111/COBI.13727, 2022.

swissALTIRegio: swissALTIRegio, https://www.swisstopo.admin.ch/en/height-model-swissaltiregio, 2025.

swissSurface3D: swissSURFACE3D, https://www.swisstopo.admin.ch/en/height-model-swisssurface3d, 2025.

Szerencsits, E.: Swiss tree lines - a GIS-based Approximation, Landscape Online, 28, 28–28, https://doi.org/10.3097/LO.201228, 2012.

Vernay, M., Lafaysse, M., Monteiro, D., Hagenmuller, P., Nheili, R., Samacoïts, R., Verfaillie, D., and Morin, S.: The S2M meteorological and snow cover reanalysis over the French mountainous areas: description and evaluation (1958–2021), Earth System Science Data, 14, 1707–1733, https://doi.org/10.5194/essd-14-1707-2022, 2022.

Vionnet, V., Brun, E., Morin, S., Boone, A., Faroux, S., Le Moigne, P., Martin, E., and Willemet, J.-M.: The detailed snowpack scheme Crocus and its implementation in SURFEX v7.2, Geosci. Model Dev, 5, 773–791, https://doi.org/10.5194/gmd-5-773-2012, 2012.

Webster, C., Essery, R., Mazzotti, G., and Jonas, T.: Using just a canopy height model to obtain lidar-level accuracy in 3D forest canopy shortwave transmissivity estimates, Agricultural and Forest Meteorology, 338, 109 429, https://doi.org/10.1016/J.AGRFORMET.2023.109429, 2023.

Webster, C., Ginzler, C., Marty, M., Nussbaumer, A., Mazzotti, G., and Jonas, T.: Hourly potential light availability maps at 10 m resolution over Switzerland, Scientific Data, 12, 1882, https://doi.org/10.1038/s41597-025-06152-9, 2025.

Winstral, A., Jonas, T., and Helbig, N.: Statistical Downscaling of Gridded Wind Speed Data Using Local Topography, Journal of Hydrometeorology, 18, 335–348, https://doi.org/10.1175/JHM-D-16-0054.1, 2017.

Xie, J., Kneubühler, M., Garonna, I., de Jong, R., Notarnicola, C., De Gregorio, L., and Schaepman, M. E.: Relative Influence of Timing and Accumulation of Snow on Alpine Land Surface Phenology, Journal of Geophysical Research: Biogeosciences, 123, 561–576, https://doi.org/10.1002/2017JG004099, 2018.

Zängl, G., Reinert, D., Rípodas, P., and Baldauf, M.: The ICON (ICOsahedral Non-hydrostatic) modelling framework of DWD and MPI-M : Description of the non-hydrostatic dynamical core, Quarterly Journal of the Royal Meteorological Society, 141, 563–579, https://doi.org/10.1002/qj.2378, 2015.